
Since January 2020 Elsevier has created a COVID-19 resource centre with free information in English and Mandarin on the novel coronavirus COVID-19. The COVID-19 resource centre is hosted on Elsevier Connect, the company's public news and information website.

Analytica Chimica Acta 1193 (2022) 339406

Contents lists available at ScienceDirect

Analytica Chimica Acta

journal homepage: www.elsevier.com/locate/aca

# Synergistic surface-enhanced Raman scattering effect to distinguish live SARS-CoV-2 S pseudovirus

Jaya Sitjar [a, 1], Hong-Zheng Xu [a, 1], Chih-Yun Liu [a, 1], Jen-Ren Wang [b, c], Jiunn-Der Liao [a, *], Huey-Pin Tsai [b, c], Han Lee [a], Bernard Haochih Liu [d], Chia-Wei Chang [e]

[a] Engineered Materials for Biomedical Applications Laboratory, Department of Materials Science and Engineering, National Cheng Kung University, Tainan, 701, Taiwan
[b] Department of Medical Laboratory Science and Biotechnology, College of Medicine, National Cheng Kung University, Tainan, 701, Taiwan
[c] Department of Pathology, National Cheng Kung University Hospital, College of Medicine, National Cheng Kung University, Tainan, 704, Taiwan
[d] Laboratory for Micro/Nanofabrication and Nanoanalysis, Department of Materials Science and Engineering, National Cheng Kung University, Tainan, 701, Taiwan
[e] MAN Technology Co. Ltd, 1F, No. 97, Yunong 3rd St., Tainan, 701, Taiwan

## HIGHLIGHTS

- Au nanocavities and Au nanoparticles on $ZrO_2$ nanobowls were used as SERS substrates to detect SARS-CoV-2 S pseudovirus.
- The SARS-CoV-2 S pseudovirus was used as the analyte for SERS-active substrates in detecting viral surface protein(s).
- Each SERS-active substrate exhibited sensitivity in detecting the characteristic SERS peaks of the SARS-CoV-2 S pseudovirus.
- The resulting peak assignment in this study can be used as a reference to distinguish the live SARS-CoV-2 virus with surface proteins.

## GRAPHICAL ABSTRACT

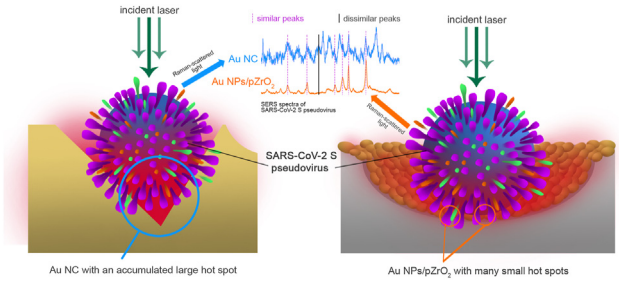


## ARTICLE INFO

*Article history:*
Received 17 November 2021
Received in revised form
17 December 2021
Accepted 24 December 2021
Available online 27 December 2021

*Keywords:*
Severe acute respiratory syndrome coronavirus 2 (SARS-CoV-2) virus
Surface-enhanced Raman spectroscopy

## ABSTRACT

The COVID-19 pandemic negatively affected the economy and health security on a global scale, causing a drastic change on lifestyle, calling a need to mitigate further transmission of the severe acute respiratory syndrome coronavirus 2 (SARS-CoV-2) virus. Surface-enhanced Raman spectroscopy (SERS) has shown great potential in the sensitive and rapid detection of various molecules including viruses, through the identification of characteristic peaks of their outer membrane proteins. Accurate detection can be developed through the synergistic integration effect among SERS-active substrate, the appropriate laser wavelength, and the target analyte. In this study, gold nanocavities (Au NC) and Au nanoparticles upon $ZrO_2$ nano-bowls (Au NPs/$pZrO_2$) were tested and used as SERS-active substrates in detecting SARS-CoV-2 pseudovirus containing S protein as a surface capsid glycoprotein (SARS-CoV-2 S pseudovirus) and vesicular stomatitis virus G (VSV-G) pseudo-type lentivirus (VSV-G pseudovirus) to demonstrate their

* Corresponding author. Engineered Materials for Biomedical Applications Laboratory, Department of Materials Science and Engineering, National Cheng Kung University, 1 University Road, Tainan, 70101, Taiwan.
*E-mail addresses:* jaya.sitjar@gmail.com (J. Sitjar), az436436@gmail.com (H.-Z. Xu), N56081527@gs.ncku.edu.tw (C.-Y. Liu), jrwang@mail.ncku.edu.tw (J.-R. Wang), jdliao@mail.ncku.edu.tw, jdliao@mail.ncku.edu.tw (J.-D. Liao), tsaihp@mail.ncku.edu.tw (H.-P. Tsai), rick594007@hotmail.com (H. Lee), hcliu@mail.ncku.edu.tw (B.H. Liu), neilschang@namliong-group.com (C.-W. Chang).
[1] The authors share an equal contribution.

https://doi.org/10.1016/j.aca.2021.339406

(SERS)
SERS-active substrate
SARS-CoV-2 S pseudovirus
Vesicular stomatitis virus G (VSV-G) pseudo-type lentivirus

virus detection capability. The optimized Au NCs and Au NPs/$pZrO_2$ substrates were then verified by examining the repetition of measurement, reproducibility, and detection limit. Due to the difference in geometry and composition of the substrates, the characteristic peak-positions of live SARS-CoV-2 S and VSV-G pseudoviruses in the obtained Raman spectra vary, which were also compared with those of inactivated ones. Based on the experimental results, SERS mechanism of each substrate to detect virus is proposed. The formation of hot spots brought by the synergistic integration effect among substrate, analyte, and laser induction may result differences in the obtained SERS spectra.



## 1. Introduction

The spread of the infectious novel coronavirus disease 2019 (COVID-19), which started on December 2020 has caused a significant negative impact on the world economy and security [1], resulting in a global urgent emergency situation that calls for efforts of public health sectors in containing further spread of the disease by thorough screening and diagnostic methods [2]. Although infected individuals show signs and symptoms of the disease, which resembles that of a common flu, e.g., fever, nasal congestion, sore throats, loss of smell and taste, etc. [3,4], it could take up to 14 days after infection for symptoms to manifest [5]. The virus is transmitted by aerosols suspended in air through coughing, sneezing, and talking; direct contact with objects contaminated with the virus has been reported to be another mode of transmission [6]. Preventive measures are thus important to minimize the number of cases, which is still rising even after a year since the start of the outbreak [7]. Screening is important to minimize the spread of the virus and is currently being done through RT-PCR and serological tests during the early and late stages of the infection, respectively [8,9] With the current development and actual implementation of vaccines, having at least the a dose of vaccine is currently being prioritized [10].

SARS-CoV-2 virus has reportedly mutated to a variety of strains which exhibit various degrees of transmissibility and infectivity [11,12]; this makes it harder to achieve the purpose of preventing infection in full effect as current mRNA-based vaccine, e.g., mainly by Pfizer/BioNTech and Moderna, modified adenovirus-based, e.g., AstraZeneca, and protein-based, e.g., Novavax, have been developed particularly against certain strains only [13]. These pharmaceutical companies have already come up with their own vaccines, each having been derived from different strains, and thus results to exhibiting different effectiveness. It has also reported in a case wherein a developed vaccine derived from D614G, an earlier mutation, was effective in neutralizing G614, which appeared later in the pandemic than D614G, demonstrating that some vaccines may be effective against multiple strains [14]. Several other mutations in the genetic makeup of SARS-CoV-2 have been reported, which tend to result to changes in infectivity and transmissibility; these mutations lead to the emergence of variants, e.g., the B.1.1.7 (Alpha), B.1.351 (Beta), B.1.617.2 (Delta), and P.1 (Gamma), variants circulating in the United States are classified as variants of concern. Some vaccines may only be significantly effective against certain variants and there is still a certain degree of uncertainty about the risk of infection, so viral infections cannot be completely avoided. As of late July 2021, the number of infected individuals did not significantly decline despite the deployment of approved vaccines, with the World Health Organization reporting 191.8 M cases worldwide. Nevertheless, vaccination offers a level of protection against the infectious disease, which can reduce further spread [15]. However, despite the availability of vaccines, screening still plays a critical role in the mitigation of disease transmission [7]. As international travel is currently severely restricted, these severe restrictions may begin to relax with the deployment of vaccines such as vaccine passport [16], but it is too early to run the risk of free movement solely on jabbing vaccines even though strict border controls requiring travelers to have been vaccinated have been implemented. Therefore, the role of the screening stage remains crucial. In addition to nucleic acid or antigen methods, a fast and accurate screening method will be the first choice to save process time [17]. Additionally, despite negative RT-PCR results and vaccination, it would be ideal if travelers undergo another round of screening through rapid testing as a confirmatory test to further ensure safety. Commercial COVID-19 test kits have started for roll out, e.g., pharmaceutical companies Roche and Lucira have developed kits for testing viral antigens and nucleic acid, respectively (Roche Diagnostics, 2021; Lucira, 2021).

Diagnostic techniques based on spectroscopy have proven capable of detecting a variety of analytes, including viruses, and even at ultra-low concentrations [17]. The technology of surface-enhanced Raman spectroscopy (SERS) is a straightforward spectroscopic method that only involves the use of a specially designed SERS-active substrate where the sample analyte is placed, and then exposed to a laser in the Raman spectrometer to obtain characteristic spectra. The characteristic spectrum of the analyte through the synergetic effect depends on the vibration mode on the surface of the analyte, which can determine the components that may be present on it [18]. In our previous work, it is possible to detect specific viruses through SERS technology by using a substrate designed specifically for the said applications. The substrate is an essential aspect to consider, and that the size of the nanostructures upon the substrate preferably matches the size of the viral analyte [19]. Some studies have combined SERS with lateral assay platforms to get the advantages of both techniques as diagnostic tools [20]. Detection of viruses needs particular handling due to its infective and transmissible nature, and so, SARS-CoV-2 should be handled in laboratories at biosafety level 3, which hinder studies involving the live virus. A study that utilized isolated N and S proteins and of SARS-CoV-2 and inactivated forms of the virus as analytes for SERS detection has provided characteristic spectra of the said proteins with the use of Au—Cu nanostars [21]. Alternatively, pseudoviruses have been developed for use as target analytes instead of using the actual highly contagious virus so that experiments utilizing live SARS-CoV-2 pseudovirus containing S protein as a surface capsid glycoprotein (SARS-CoV-2 S pseudovirus) could be carried out in a laboratory with lower biosafety level.

An in-depth investigation with the applicability of SERS in detecting SARS-CoV-2 could demonstrate its potential as a biosensor not only to the current pandemic situation but could even be considered as a tool for future outbreaks. In this study, a SARS-CoV-2 S pseudovirus is used to study the effectiveness of particularly designed SERS-active in screening SARS-CoV-2 S pseudovirus. In order to obtain the characteristic SERS spectrum of the SARS-CoV-2 S pseudovirus, two types of SERS-active substrates,

namely Au nanocavities (Au NC) and Au nanoparticles on the porous $ZrO_2$ (Au NPs/p$ZrO_2$) are fabricated and used to distinguish SARS-CoV-2 S pseudovirus and vesicular stomatitis virus G (VSV-G) pseudo-type lentivirus (VSV-G pseudovirus). A synergetic effect between two substrates that are competent to detect the viruses is thereafter discussed and compared. This study is anticipated to explore the possibility of applying SERS technique as a potential diagnostic tool; however, succeeding studies would be necessary to further investigate the applicability of the technique in clinical settings.

## 2. Experimental section

### 2.1. Fabrication of SERS-active substrates

#### 2.1.1. Au NC

Au NCs were prepared firstly through the thermal evaporation of ~100 nm thick Au (99.99% purity) onto cleaned Si wafers primed with ~5 nm thick titanium adhesion layer. Nanocavities were then formed on the surface of the Au-coated Si with a nano indenter equipped with a dynamic contact module and nano-vision system (NanoIndenter G200, Agilent technologies, USA), with a diamond *Berkovich* indenter tip with a radius of ~20 nm. Parameters that were maintained throughout the experiment were drift rate (0.05 nm/s), strain rate (0.1/s), approaching velocity (1 nm/s), harmonic displacement (1 nm), humidity (32%), and temperature (24 °C). Indentation depth ($I_d$) and tip-to-tip displacement ($I_{t\text{-}t}$) were set at 100, 120, and 140 nm and 520, 600, and 700 nm, respectively, these are denoted by Au NC ($I_d$-$I_{t\text{-}t}$).

#### 2.1.2. Au NPs/p$ZrO_2$

Polystyrene nanoparticles (PS NPs) of diameters ($D_P$ = 150, 250, and 350 nm) were deposited onto cleaned Si substrates and were slightly annealed at 50 °C for 10 min before spin-coating with a precursor solution of $ZrO_2$. The $ZrO_2$ precursor was prepared with a mixture of zirconium tetrachloride ($ZrCl_4$, 98%, Acros Organics, Pittsburgh, PA, USA) and isopropanol (99.8%, Panreac Applichem, Darmstadt, Germany) that was left to stand for ~24 h until it achieved a gel-like consistency before use for spin-coating. $ZrO_2$ was then allowed to form on the surface of the coated samples through annealing at 600 °C for 3 h to remove the template layer of PS NPs, leaving behind a regularly arranged concave porous $ZrO_2$. With the use of an electron beam evaporator, Au NPs were deposited onto the porous $ZrO_2$ substrate to produce SERS-active Au NPs/p$ZrO_2$ substrates. As Au NPs/p$ZrO_2$ substrates were fabricated at three varying PS NP sizes, resulting to a variation in the depth, pore, and pore wall sizes, these are denoted by Au NPs/p$ZrO_2$ ($D_P$).

#### 2.1.3. Calculation of enhancement factor (EF)

Rhodamine 6G (R6G) was chosen as the molecular probe in the determination of the enhancement factor exhibited by each substrate. R6G solution with a concentration of $10^{-3}$ M was dropped onto the substrate and allowed to dry in air at room temperature before subjecting to Raman spectroscopy at an excitation wavelength of 633 nm. The EF was calculated based on the standard equation as shown:

$$EF = \frac{I_{SERS}}{I_{bulk}} \times \frac{N_{bulk}}{N_{SERS}} \quad \text{Equation (1)}$$

where $I_{SERS}$ and $I_{bulk}$ are intensities of characteristic peaks that correspond to the SERS and normal Raman conditions while $N_{SERS}$ and $N_{bulk}$ are the estimated number of molecules that participate in the SERS and normal Raman scattering, respectively.

### 2.2. Morphology and composition of SERS-active substrates

High-resolution thermal field emission scanning electron microscope coupled with energy dispersive X-Ray spectroscopy (FE-SEM/EDS, JSM-7000, JEOL, Tokyo) and atomic force microscope (AFM, Dimension Icon, Bruker, Karlsruhe, Germany) were utilized to analyze the morphology and composition of the SERS-active substrates. Images were taken at secondary electron imaging mode at an accelerating voltage of 10 kV.

### 2.3. Preparation of SARS-CoV-2 S pseudovirus

SARS-CoV-2 S pseudovirus was produced following the report of Huang et al. with minor modifications (Huang et al., 2020). The lentiviral vector system was provided by the National RNAi Core of Academia Sinica Taiwan. De novo synthesis was performed to obtain sequences of the spike protein, which were then cloned into the pMD.G plasmid to express SARS-CoV-2 S pseudoviruses. Cells were transfected with a total of 40 μg pCMVdeltaR8.91, pLAS3w and pMD.G (VSV-G pseudo-type lentivirus, or VSV-G pseudovirus) or pcDNA3.1-spike Wuhan plasmids (SARS-CoV-2 S pseudovirus). A brief illustration on the outer membranes of SARS-CoV-2 S and VSV-G pseudoviruses, and live SARS-CoV-2 virus is shown in Supporting Data (SD) 1.

### 2.4. Detection of SARS-CoV-2 S pseudovirus: repetition of measurement and reproducibility

With the use of the fabricated Au NC and Au NPs/p$ZrO_2$ substrates, SERS experiments were performed with the use of the Raman spectrometer (UniDRON, CL Technology Co. Ltd.) with a chosen laser source of 633 nm for virus analytes and a maximum laser power of 35 mW. The pseudovirus sample was dropped onto the substrate and then covered with a glass cover slip before subjecting to the Raman laser for measurement. In this experiment, spectra were taken five times on the same spot of the substrate to investigate the effect of exposing the same area on the change of peak intensities, and six different locations on the same nanostructures array were tested to see the reproducibility of results and consistency of the SERS spectra.

### 2.5. Detection of SARS-CoV-2 S pseudovirus: about limit of detection

The SARS-CoV-2 S pseudovirus was also prepared at varying dilutions $10^{-1}$, $10^{-2}$, and stock to investigate the change in the peak intensities in both substrates, with the change in the concentration of the analyte. The same Raman spectrometer settings as mentioned above were applied in the collection of spectra in this investigation. Six different locations on the same nanostructures array were averaged.

### 2.6. Inactivation methods for live SARS-CoV-2 S pseudovirus

Aside from live SARS-CoV-2 S pseudovirus, the SERS spectra of live VSV-G pseudovirus and inactivated SARS-CoV-2 S pseudovirus inactivated through thermal inactivation and autoclave were also obtained using both Au NC and Au NPs/p$ZrO_2$. Subtracted spectra from these pseudoviruses were then taken to determine the peaks that are unique to the pseudoviruses, indicating the possible functional groups present on the surfaces of their membranes. Six different locations on the same nanostructures array were averaged.

## 3. Results and discussion

### 3.1. Substrates of Au NC and Au/pZrO$_2$

In this section, based upon our previous review [17], surface morphology and cross-sectional profile and SERS property of both substrates are evaluated in order to choose size-matching substrates for detecting the target analyte, SARS-CoV-2 S pseudovirus.

#### 3.1.1. Surface morphologies and cross-sectional profiles

SEM and AFM images of Au NCs and Au NPs/pZrO$_2$ in different sizes and dimensions were shown in Fig. 1(a), (b), and SD 2. In Fig. 1 (a-1), SEM image of Au NC (120–600) was shown. The other images from different samples with varied $I_d$ and $T_{t\text{-}t}$ were also shown in SD 2. In Fig. 1 (a-2), AFM image of Au NC feature a mound-like structure arranged in a diagonal array as a result of cavity-formation of a triangular *Berkovich* nanoindenter tip. It is also shown through the cross-sectional profile (~700 nm) that the measured depth of Au NC with the AFM tip is ~50 nm, which is lower than the expected $I_d$ = 120 nm used in Au NC (120–600). Note that current AFM tip is incapable of reaching the entire depth of the cavities, thus the measured depth is limited, as compared with the expected value, shown as the dotted lines.

In Fig. 1 (b), SEM and AFM images of Au NPs/pZrO$_2$ (250) were shown. The images shown feature a concave bowl-like structure arranged in a hexagonal array. Through cross-sectional profiling (~700 nm), the as-formed nano-bowls exhibit depths of 60–80 nm and widths ranging from 240–250 nm, corresponding to the $D_P$ of the PS NPs used in fabricating Au NPs/pZrO$_2$ (250), as seen in Fig. 1 (b-2) and 1 (b-3). Au NPs deposited onto the ZrO$_2$ nano-bowls take on a flattened form and create clusters that measure around 30–60 nm wide and <10 nm thick. Thus, the diameter of the nano-bowl is ~240 nm, taking into consideration the thickness of the deposited Au NP clusters. Au NPs were deposited on the ZrO$_2$ nano-bowls and distributed in clusters. The other images from Au NPs/pZrO$_2$ with varied $D_P$ were also shown in SD 2.

#### 3.1.2. SERS enhancement factor

The EFs of Au NC and Au NPs/pZrO$_2$ were estimated, by equation (1), to be $5.5 \times 10^7$ and $4.3 \times 10^7$, respectively, which are comparable to averaged values relative to recently developed SERS-active substrates (Chang et al. [1], 2011; Sitjar et al., 2019). Since the geometry of the nanostructure is a critical factor affecting the overall performance of the SERS-active system, it varies with the cavity and pore size of Au NCs and Au NPs/pZrO$_2$ and provides information on how SERS affects the overall test results through size matching.

### 3.2. Optimal parameters for SERS measurements

In this section, the applicability of two size-matching substrates, Au NCs (120–600) and Au NPs/pZrO$_2$ (250), and the use of live SARS-CoV-2 S pseudovirus at as-received concentration using as the analytes are evaluated. Four tests are measured, and results are discussed in the following sections.

#### 3.2.1. Limit of detection factor

In the study of SARS-CoV-2 S pseudovirus at varying dilutions, with results shown in SD 3, distinct sharp peaks, as listed in Table 1 for Au NC and Au NPs/pZrO$_2$, could be observed with the stock solution; however, upon further dilution, the peaks weaken. In the case of Au NC (120–600), distinct peaks are still observable at $10^{-1}$ dilution, whereas an almost flat spectrum is shown at $10^{-2}$ dilution. It may indicate the probability, rather than the concentration, of detecting virus particles in the nanostructures at e.g., $10^{-1}$ dilution. In the case of Au NPs/pZrO$_2$ (250), the peaks at $10^{-1}$ and $10^{-2}$ dilution were not as distinct as that in Au NC (120–600) and instead, a strong background can be observed. It shows the characteristics of SERS-active substrate with respect to the detected analyte in a diluted condition, e.g., in the cases at $10^{-1}$ and lower. Note that one Raman spot (e.g. with a diameter of 1 μm) may cover a few nanostructures (e.g., ~5 for Au NC (120–600) and ~11 for Au NPs/pZrO$_2$ (250)), which accommodate a limited quantity of virus particles.

In our previous studies (Chang et al. [23]; Sitjar et al. [22]), by taking these two substrates in measuring physically adsorbed R6G

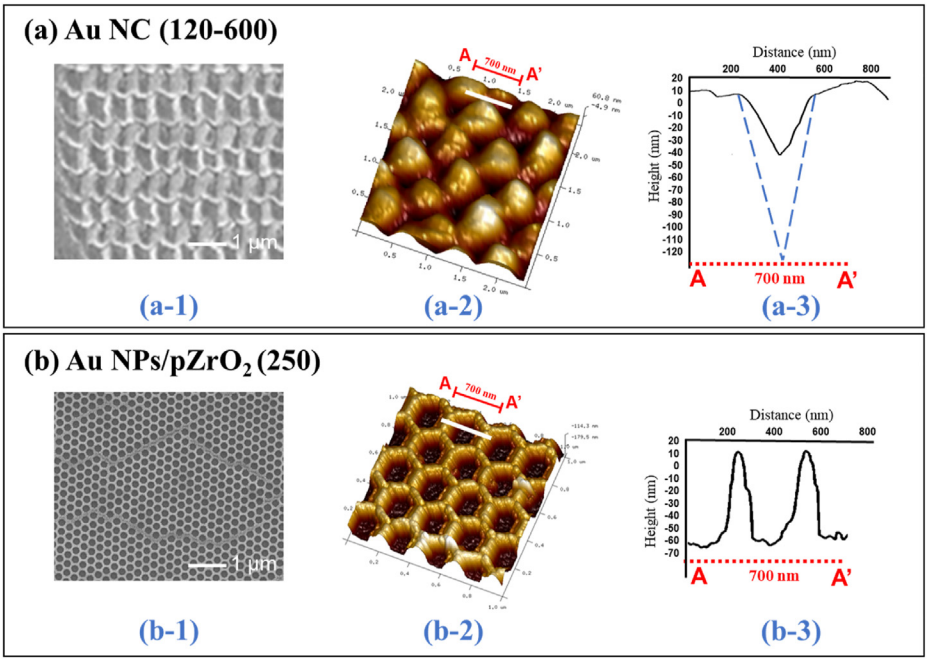


**Fig. 1.** Surface morphologies of (a) Au NC (120–600) and (b) Au NPs/pZrO$_2$ (250 nm) shown by SEM photo-images (a-1 and b-1), AFM topographies (a-2 and b-2), and cross-sectional profiling (a-3 and b-3), respectively.

**Table 1**
SARS-CoV-2 S and VSV-G pseudoviruses - peaks obtained from this study and the references (only for VSV-G pseudovirus) their corresponding peak assignments ($cm^{-1}$).

| SARS-CoV-2 S pseudovirus - peaks obtained from this study | Peak assignment | VSV-G pseudovirus - peaks obtained from this study | Peak assignment | Reference (only for VSV-G pseudovirus) |
|---|---|---|---|---|
| 837[a]/830[b] | Ring breathing/Fermi doublet in Tyrosine | 1164 | C=C stretching in lipids/proteins | De Gelder et al. |
| 1007[a,c]/1000–1003[b] | Symmetric ring breathing in Phenylalanine | 1358 | Tryptophan | Movasaghi et al. |
| 1100[a] | Proline, Alanine | 1506 | N–H bending | Chen et al. |
| 1237[a,c]/1240–1243[b] | Amide III (β-strand) | | | |
| 1305-1306[a,b,c] | Amide III (α-helix) | 1548 | C=N stretching in dCTP | Chen et al. |
| 1358[a]/1355[b] | Ring breathing in Tryptophan | 1598 | C–N stretching of N-formyl group in N′-formylkynurenine; Ring vibrations in tyrosine | Jyothi Lakshmi et al. |
| 1506[a]/1507[b] | C–N stretching mode in dATP | 1648 | Amide I in α-helix | Tuma et al. |

[a] indicates characteristic peaks obtained with Au NC (120–600).
[b] indicates characteristic peaks obtained with Au NPs/$pZrO_2$.
[c] indicates peaks that are common to this study and with that of (Carlomagno et al., 2021) using COVID-19 infected saliva samples.

and pesticide molecules in solution, calibration plots produced by the linear trend in the logarithmic scale between the 1360 $cm^{-1}$ peak intensities and concentrations were obtained. The limit of detection for the probe molecules could reach to a very small quantity. For current virus detection, it is still required to study the correlation between the probability of detecting relatively large virus particles in the nanostructures and the method to dilute the as-received concentration of the virus sample.

### 3.2.2. Applied laser power factor

Laser power may affect the resulting SERS effect (Sitjar et al., 2021) - too high may damage the virus sample, and too low may not induce energy to provide a strong enough signal for analyte identification. SERS spectra obtained at varying laser powers with the use of both substrates were shown in SD 4. Results of experimentation lead to a selection that the optimal Raman laser power to detect the pseudovirus in both Au NC and Au NPs/$pZrO_2$ substrates is ~3.5 mW, which is ~10% of the full power of the instrument that was utilized. Although peaks appeared to be intense at full laser power, some peaks appeared to be more distinguishable when a laser power of 3.5 mW was used, implying that a full power might have caused sample degradation. Since biological samples are feeble and sensitive to external energy sources [24], pseudoviruses are delicate due to their organic biomolecular compositions that could easily deteriorate upon exposure to high energy and harsh conditions.

### 3.2.3. Measurement times factor

SERS spectra obtained from using the same substrate location with five consecutive times are shown in SD 5. SERS spectra remain consistent with both substrates, showing the same characteristic peaks, as listed in Table 1 and marked in SD 5 (a-1) and (b-1), at the same Raman shifts throughout five measurements, but with a decline in intensities with the increasing use of the same substrate spot (from 1st to 5th accumulation). This decline in intensities is due to a potential damage caused by the laser to both the substrate and the analytes by the continuous use of the same spot, as presented in SD 5 (a-2) and 2 (b-2). Although three characteristic peaks (837/830, 1007/1002, 1358/1355 $cm^{-1}$) appear in both Au NC and Au NPs/$pZrO_2$ substrates, the remaining peaks differ – the differences in the appearance of peaks may be caused by the difference in substrate geometry and composition.

As shown in SD 5 (b), all characteristic peaks using the Au NC (120–600) appear to exhibit a slight decrease in intensities with succeeding accumulations, followed by a noticeable drop in the intensities at the 5th accumulation. In the case of Au NPs/$pZrO_2$ (250), the intensities of the characteristic peaks follow a gradual decrease with succeeding accumulations. Both of these substrates are still capable of detecting the pseudovirus even after five measurements on the same spot, though a clearer spectrum with distinctive strong peaks can be observed as one measurement is used to avoid degradation of the analyte in the substrate.

### 3.2.4. Substrate repeatability factor

SERS spectra obtained at 6 different locations on the two substrates are shown in Fig. 2 (a) and (b). The characteristic peaks, as indicated in Table 1, are strong regardless of location. Note that peaks shifting on Au NPs/$pZrO_2$ (250) are mostly likely caused by the clustered arrangement of NPs on the $pZrO_2$ substrate. In the cases of both substrates, all peaks in all six locations consistently appear with only slight deviations in the intensities, as plotted in SD 6 (a) and (b). Aside from geometrical deviations, the appearance of peaks in a SERS spectrum may also be dependent on how analyte molecules are oriented with respect to the accommodated nanostructure. Since pseudoviruses are relatively large biomolecules, it is likely that some of the functional groups may only reflect as weak peaks or not appear at all in the event that these functional groups in particular are not within the range of the strongest hot spot area/s in the nanostructure [25].

Both substrates show consistency in the characteristic peaks with their respective resulting SARS-CoV-2 S pseudovirus spectra. There could be notable differences in the intensities with varying locations such as in the case of Au NPs/$pZrO_2$ (250). Au NPs/$pZrO_2$ is fabricated through multiple steps with the formation of $ZrO_2$ pores by sol-gel and deposition of Au NPs; along the fabrication process, some of the structures that were formed in previous steps may have been compromised in the subsequent steps due to handling and processing, which could have affected the uniformity of nanostructures. On the other hand, the fabrication process to produce Au NC involves a simple indentation step after deposition of Au film. It does not go through multiple steps, lowering the chances of sample damage, which could explain that intensities of the peaks with Au NC (120–600) are more consistent than in Au NPs/$pZrO_2$ (250). Nevertheless, both substrates are capable of detecting the pseudovirus; however, for Au NPs/$pZrO_2$ (250), multiple measurements in varying locations should be done to ensure that the resulting peaks do belong to the analyte of interest.

## 3.3. Live and inactivated SARS-CoV-2 S pseudoviruses

In this section, a comparison between live SARS-CoV-2 and VSV-G pseudoviruses from where it is derived is discussed. Additionally,

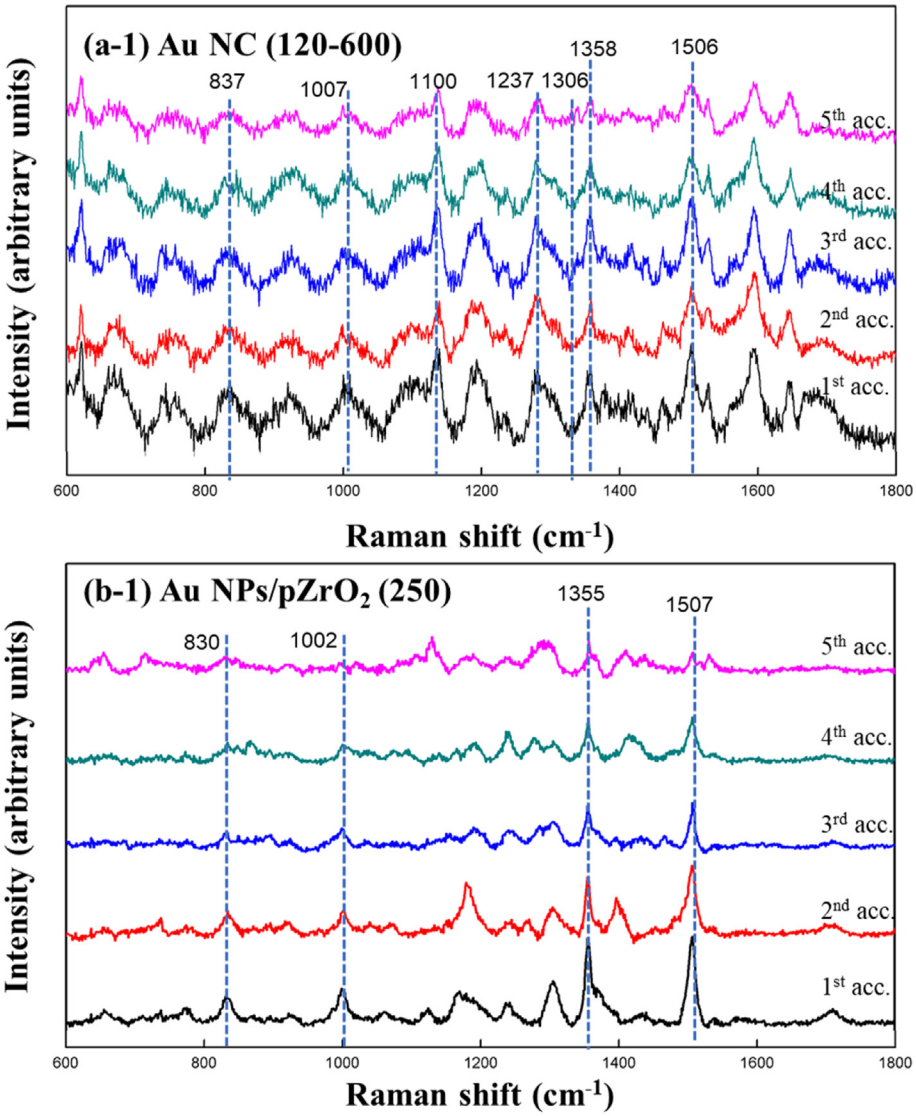


**Fig. 2.** SERS spectra of SARS-CoV-2 S pseudovirus taken at six different locations (loc. 1–6) on the same substrate: (a) Au NC (120–600) and (b) Au NPs/pZrO$_2$ (250 nm), with relative intensities of characteristic peaks on SD 6 (a) and (b). No significance of relative intensities among different locations was found.

live SARS-CoV-2 S pseudovirus is inactivated through various methods and their resulting SERS spectra are analyzed to observe the changes in the peak shifts and intensities.

### 3.3.1. Live and damaged viruses

In Fig. 3, a comparison to detect SARS-CoV-2 S with VSV-G pseudoviruses using the two substrates is shown. Since the components of VSV-G pseudovirus is known as it is widely studied, it could serve as a reference to SARS-CoV-2 S pseudovirus to determine the peaks that belongs to SARS-CoV-2 S pseudovirus. The SERS spectra of both pseudoviruses are shown in the figure as well as the corresponding subtracted spectra. Obtained peaks and their peak assignments are listed in Table 1.

Although it is different in using the analyte, a recent study [26] has demonstrated the possibility of detecting SARS-CoV-2 virus from saliva samples with a Raman-based approach (i.e., a non-SERS-active substrate). By analyzing the samples to discriminate the signal of patients with a current infection by COVID-19 from healthy subjects and/or subjects with a past infection, the differences in saliva biochemical composition can be specified. As shown in the reference [26], peaks corresponding to phenylalanine (1000 cm$^{-1}$) and amide III (1249 and 1317 cm$^{-1}$) are common to the results of this study, i.e., 1007, 1237, 1305-1306 cm$^{-1}$ for Au NC and 1000–1003, 1240–1243, and 1305-1306 cm$^{-1}$ for Au NPs/pZrO$_2$. These two functional groups may belong to some of the components of the spike protein in SARS-CoV-2 S virus. Additionally, the functional groups listed in Table 1 correspond to the groups present on the surface of the detected virus particles, as illustrated in SD 1, which most likely resemble to the components of the S-glycoprotein, such as phenylalanine and amide groups [27].

### 3.3.2. Live SARS-CoV-2 and VSV-G pseudoviruses

The subtracted spectra represented the subtraction of the VSV-G pseudovirus spectra from the SARS-CoV-2 S pseudovirus spectra; the positive peaks on the subtracted spectra then correspond to peaks of SARS-CoV-2 S pseudovirus, while the negative peaks are that of the VSV-G pseudovirus. Referring to Fig. 3 (a), the subtracted spectra obtained from using the Au NC (120–600) exhibited

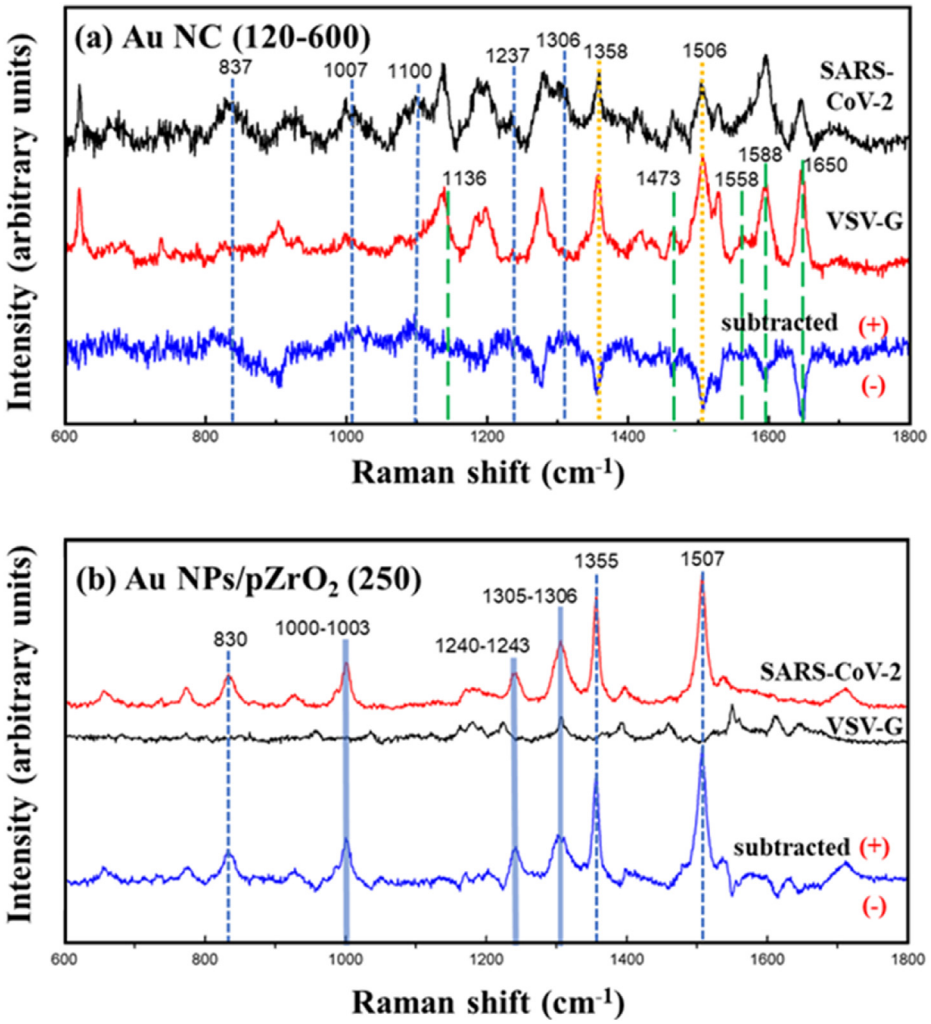


**Fig. 3.** SERS spectra of SARS-CoV-2 S and VSV-G pseudovirusses and their subtracted curves using (a) Au NC (120–600) and (b) Au NPs/$pZrO_2$ (250) as the substrates; considering the subtracted spectra, (+) positive peaks indicate peaks that are higher in intensity with SARS-CoV-2 S pseudovirus than that with VSV-G pseudovirus, while (−) negative peaks correspond to peaks higher in intensity with VSV-G than SARS-CoV-2 S pseudovirus. The characteristic peaks are respectively assigned in Table 1: short-dashed blue lines are respectively related to SARS-CoV-2 S pseudovirus, solid yellow lines for peaks that apprear more intense in VSV-G than those in SARS-CoV-2 S, and long-dashed green lines for peaks that appear in both virus analytes at intensities that are almost the same. (For interpretation of the references to colour in this figure legend, the reader is referred to the Web version of this article.)

stronger negative peaks than positive ones, which on the other hand, is not the case with Au NPs/$pZrO_2$ (250) as show in Fig. 3 (b). Both substrates may be capable of detecting the pseudoviruses, but it appears that more distinctive signals of the SARS-CoV-2 S pseudovirus can be obtained through Au NPs/$pZrO_2$. Peaks at 1164, 1358, 1506, 1598, and 1648 $cm^{-1}$ can be observed in both SARS-CoV-2 S and VSV-G pseudovirus with Au NC (120–600) but not in the case of Au NPs/$pZrO_2$, as shown in Fig. 3. Both substrates differ in geometry and are expected to give different results; peaks that might be enhanced in one substrate may not exhibit in the same degree of enhancement as with the other substrate. Since the SARS-CoV-2 S pseudovirus was derived from the VSV-G pseudovirus, it is expected that both analytes would exhibit common peaks, which are shown in Table 1 and Fig. 3. Additionally, since the SARS-CoV-2 S pseudovirus was derived from the VSV-G pseudovirus, they only differ in a part of the surface proteins. The corresponding assignments to these peaks may belong to components of the glycoproteins unique only to VSV-G pseudovirus (SD 1 (3)). Generally, peak intensities for VSV-G pseudovirus in Au NPs/$pZrO_2$ (250) are weaker compared to those in Au NC (120–600), wherein peaks intensity at 1548 and 1648 $cm^{-1}$ for VSV-G pseudovirus are even much stronger than those in SARS-CoV-2 S pseudovirus. This implies that the substrate effect and the number of analytes in the nanostructure (i.e., to form the hot spot(s)) are involved in the enhancement of peaks.

Additionally, SERS spectra of the live and inactivated SARS-CoV-2 S pseudovirus were also obtained and are shown in Fig. 4. As expected in all substrates, comparing to the spectra of the live pseudovirus, less intense peaks are seen with the inactivated pseudovirus, but peaks are still distinguishable. Notably, as shown in Fig. 4 (a), using Au NC (120–600) with pseudovirus that has been thermally inactivated at 65 °C and inactivated with UV, all of the characteristic peaks are still relatively intense indicating that these inactivation methods do not completely modify the composition of the pseudovirus. On the other hand, with the spectrum of that of autoclaved sample did not exhibit distinguishable peaks at all. However, as with Au NPs/$pZrO_2$ in Fig. 4 (b), the intensities of the characteristic peaks appeared to have weakened with all inactivation methods applied. Therefore, based on these experiments, it is observed that both substrates were able to demonstrate detection

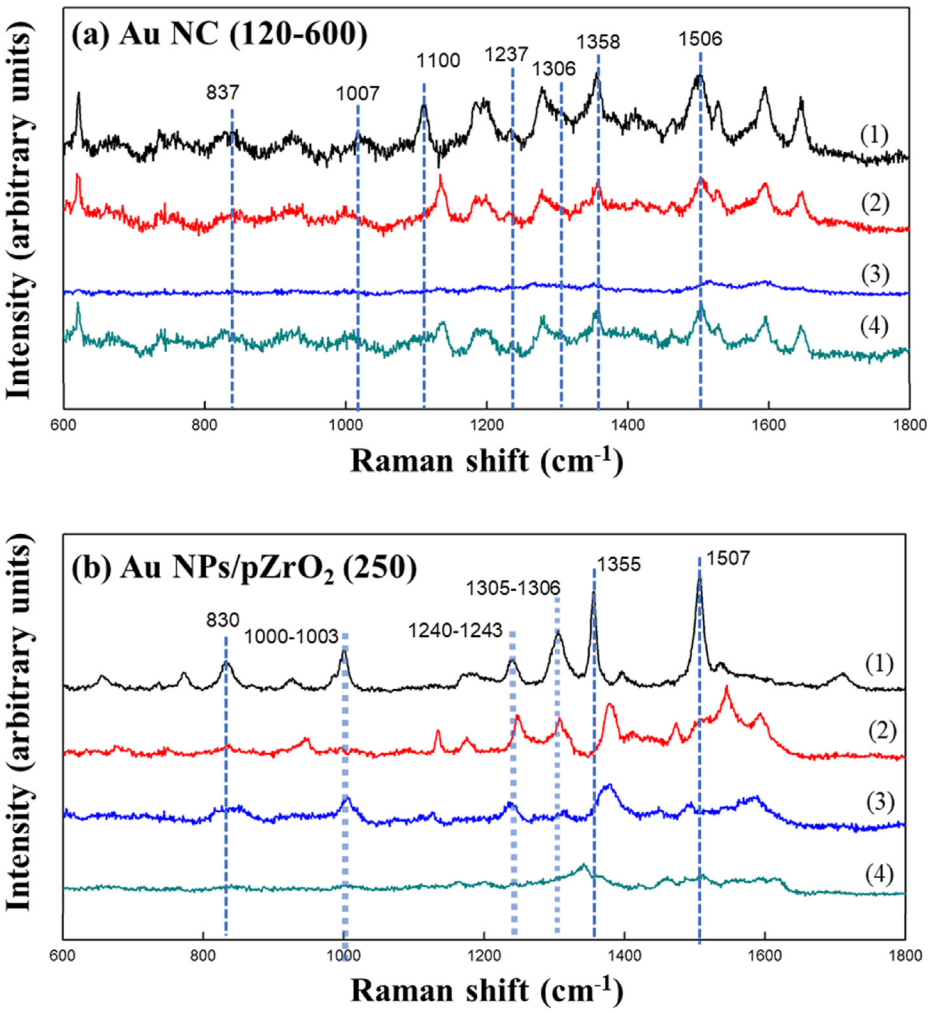


**Fig. 4.** SERS spectra of SARS-CoV-2 S pseudovirus – (1) live and inactivated viruses by different methods: (2) 65 °C heating for 30 min, (3) autoclave for 20 min, and (4) UV irradiation for 30 min; two substrates (a) Au NC (120–600) and (b) Au NPs/$pZrO_2$ (250) were used.

of pseudoviruses at full and partial damage. Partial damage was observed with weakened peak intensities in comparison to the peaks observed with the live viruses, while full damage was observed with complete disappearance of characteristic peaks.

In the case of Au NC (120–600), it is seen that full damage on the autoclaved pseudovirus was detected, while for Au NPs/$pZrO_2$, it was the same for the UV irradiated sample. Additionally, different results have been obtained from both substrates. It implies that an in-depth insight with regards to the suitability of each substrate in detecting an inactivated form of a live virus is required.

### 3.4. Mechanisms of SARS-CoV-2 S pseudovirus detection

SERS-active substrates are driven by mechanisms based predominantly on their geometry (i.e., electromagnetic mechanism) and a minor contribution from chemical interactions (i.e., chemical mechanism) between the analyte and its immediate surrounding environment. In this section, these mechanisms are considered with respect to the geometry exhibit by each substrate, showing how hot spots are formed and how these hot spots are positioned relative to the pseudovirus analytes.

#### 3.4.1. Substrate effect

In the case of this study, the analytes and laser conditions remained the same throughout the experiments, varying only on the type of substrate. Thus, Fig. 5 shows the difference in the resulting electromagnetic mechanism as a consequence of the difference in geometry. Top views of each substrate with virus particle/s are shown in Fig. 5(a), (c-1), and (c-2). The Au NC features a cavity that is sharp and gets narrower as it goes deeper into the substrate (Fig. 5(b)); the Au/$pZrO_2$ on the other hand, features a bowl-like structure that gets wider with depth as in Figs. 5(d-1). The average cavity diameter in Au NC is ~200 nm, but due to the narrow space of the cavities and given that the pseudovirus measures ~100 nm, a single cavity could hold one pseudovirus (i.e., as effectively measured) while one bowl-like structure of Au/$pZrO_2$ (250) could hold up to 3 pseudoviruses (i.e., equally placed as shown in Figs. 5(c-1)) due to it being wider, having more capacity than Au NC. It is also important to note that the spacing between the Au NP clusters were found to be at a few nanometers (<10 nm), where hot spots are formed. Comparing how the analytes are positioned with respect to the nanostructures, as in Fig. 5(b), (d-1), and (d-2), analytes in Au NC is exposed to a stronger electromagnetic field, and in consequence, stronger hot spots, due to the sharp edges found in the cavities.

Moreover, as shown in Fig. 5 (c-2) and (d-2), in the case wherein a single virus particle is centered on a nanostructure, there are free spaces on the border of the structure for more virus particles to be

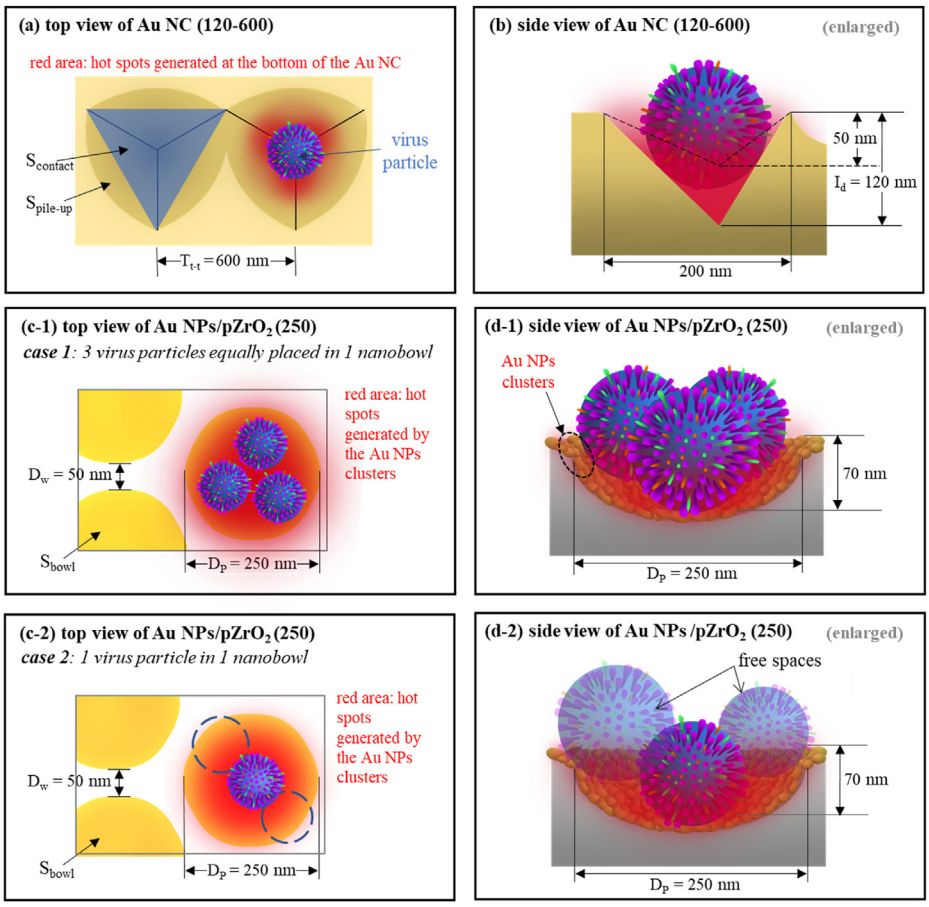


**Fig. 5.** Suggested mechanisms for the detection of SARS-CoV-2 S pseudovirus: (a) top and (b) cross-sectional side-views of Au NC with one possibly fitted virus analyte and (c-1 and c-2) top and (d-1 and d-2) cross-sectional side-views of Au NPs/$pZrO_2$ with possibly fitted virus analytes in e.g., 2 cases, to show their relative sizes and dimensions. The virus analyte without contact with Au NPs clusters in (c-2) and (d-2) is expressed as free space. In (a), $S_{contact}$ denotes the surface area in contact with the nanoindenter tip, while $S_{pile-up}$ is the surface area of the material pile-up as a consequence of the indentation process. In (c-1) and (c-2), $S_{bowl}$ is the surface area of the nano-bowl while $D_w$ represents the distance between the nano-bowls.

situated in, but are exposed to hot spots that are weaker than those located at the bottom of the nanostructure, forming a collective effect with Au NPs clusters [22].

### 3.4.2. *Influence of the synergetic effect*

The performance of small hot spots formed by Au NP clusters on Au NPs/$pZrO_2$ may be varied with the amount accommodated virus particles and dependent on the collective result of small hot spots. It exhibits different from the case of Au NC that the entire surface of the cavity is uniformly covered by Au film and formed a unique and large hot spot under the analyte. For Au NPs/$pZrO_2$, $ZrO_2$ component contributes a chemical enhancement effect, but does minor relative to the electromagnetic enhancement induced by plasmonic components [22].

## 4. Conclusion and perspectives

The uses of Au NC (120−600) and Au NPs/$pZrO_2$ are explored to test the capability of detecting SARS-CoV-2 S pseudovirus as a study to eventually detect live SARS-CoV-2 virus. Optimal combinations of laser wavelength and SERS-active substrate are determined to obtain conditions that are suitable for detecting the said pseudoviruses. Moreover, the substrates also show the capability to detect inactivated forms of the pseudovirus. Although both substrates differ in terms of geometry and composition, they provide characteristic SERS spectra of the same analyte. It is very likely that the specific morphology and composition of each substrate could enhance particular peaks, in addition to the fact that orientation of analytes on the outer membrane protein upon the nanostructures could also affect the resulting spectra. Moreover, with the detection of a relatively large molecule such as the pseudovirus, a nanostructure provides a large hot spot such as Au NC (120−600) to match the analyte size is competent to maximize the exposure of the virus surface to the hot spot. On the other hand, a nanostructure with many small hot spots such as Au NPs/$pZrO_2$ (250) also exhibits the ability to distinguish peaks characteristic to pseudovirus. The resulting plasmonic hot spots of each substrate also differ in terms of intensity and geometry, which could also be a factor that should be considered in explaining this variation in SERS spectra. Considering all of the measurement factors, i.e., substrate geometry and composition, laser wavelength and power, and analyte, the overall effects of their synergy would bring dissimilarities in SERS spectra with the variations of these parameters. Moreover, both substrates exhibit detection capabilities but operate in different SERS mechanisms due to the differences in the substrate design.

This study explores the capability of SERS as a potential tool in the diagnosis of infectious viruses such as SARS-CoV-2 virus and its variants. The use of SARS-CoV-2 S pseudovirus as the target analyte in this study was to demonstrate that the fabricated SERS-active substrates can be used to obtain characteristic SERS spectra to

relate to the peaks of the SARS-CoV-2 S protein. Actual live SARS-CoV-2 virus, with two more proteins, could then be used in the succeeding future studies, e.g., the assigned peaks obtained in this study could be used as a reference. Moreover, actual samples with the inclusion of saliva and nasopharyngeal swabs can be furthermore considered to investigate the applicability of the technique to clinical applications.

## CRediT authorship contribution statement

**Jaya Sitjar:** Writing – original draft, Writing – review & editing. **Hong-Zheng Xu:** Methodology, Data curation. **Chih-Yun Liu:** Methodology, Data curation. **Jiunn-Der Liao:** Supervision, Writing – review & editing, Conceptualization. **Han Lee:** Writing – review & editing. **Chia-Wei Chang:** Conceptualization.

## Declaration of competing interest

The authors declare the following financial interests/personal relationships which may be considered as potential competing interests: Jiunn-Der Liao reports financial support was provided by Republic of China Ministry of Science and Technology. Jiunn-Der Liao has patent pending to National Cheng Kung University.

## Acknowledgements

This work was supported by the Ministry of Science and Technology of Taiwan (grant numbers: MOST 109-2224-E-006-008, 109-2327-B-006-005, 110-2221-E-006-0144-MY3, and 109-2811-E-006-531-MY2), The BSL-3 Virology Laboratory of National Cheng Kung University Hospital, Tainan, Taiwan (with authorization), and Center for Drug Evaluation (CDE) of Taiwan (case number: 109IDX08030). We also thank Ms. Yun-Yin Lien for the preparation of pseudoviruses for this study. The authors declare no conflict of interest.

## References

[1] S. Mehta, T. Saxena, N. Purohit, The new consumer behaviour paradigm amid COVID-19: permanent or transient? J. Health Manag. 22 (2020) 291–301, https://doi.org/10.1177/0972063420940834.
[2] O. Belmehdi, M. Hakkour, N. El Omari, A. Balahbib, F.E. Guaouguaou, T. Benali, A. El Baaboua, M. Lahmoud, N. Elmenyiy, A. Bouyahya, Molecular structure, pathophysiology, and diagnosis of COVID-19, Biointerface Res. Appl. Chem. 11 (2021) 10215–10237, https://doi.org/10.33263/BRIAC113.1021510237.
[3] F. Heidari, E. Karimi, M. Firouzifar, P. Khamushian, R. Ansari, M.M. Ardehali, F. Heidari, Anosmia as a prominent symptom of COVID-19 infection, Rhinology 58 (2020) 302–303, https://doi.org/10.4193/Rhin20.140.
[4] T. Klopfenstein, N.J. Kadiane-Oussou, L. Toko, P.Y. Royer, Q. Lepiller, V. Gendrin, S. Zayet, Features of anosmia in COVID-19, Med. Maladies Infect. 50 (2020) 436–439, https://doi.org/10.1016/j.medmal.2020.04.006.
[5] A.G. Hadi, M. Kadhom, N. Hairunisa, E. Yousif, S.A. Mohammed, A review on COVID-19: origin, spread, symptoms, treatment, and prevention, Biointerface Res. Appl. Chem. 10 (2020) 7234–7242, https://doi.org/10.33263/BRIAC106.72347242.
[6] M. Lotfi, M.R. Hamblin, N. Rezaei, COVID-19: transmission, prevention, and potential therapeutic opportunities, Clin. Chim. Acta 508 (2020) 254–266, https://doi.org/10.1016/j.cca.2020.05.044.
[7] K.M. Gostic, A.C.R. Gomez, R.O. Mummah, A.J. Kucharski, J.O. Lloyd-Smith, Estimated effectiveness of symptom and risk screening to prevent the spread of COVID-19, Elife 9 (2020) 1–18, https://doi.org/10.7554/eLife.55570.
[8] A. Tahamtan, A. Ardebili, Real-time RT-PCR in COVID-19 detection: issues affecting the results, Expert Rev. Mol. Diagn. 20 (2020) 453–454, https://doi.org/10.1080/14737159.2020.1757437.
[9] B. Giri, S. Pandey, R. Shrestha, K. Pokharel, F.S. Ligler, B.B. Neupane, Review of analytical performance of COVID-19 detection methods, Anal. Bioanal. Chem. (2020), https://doi.org/10.1007/s00216-020-02889-x.
[10] W.G. dos Santos, Impact of virus genetic variability and host immunity for the success of COVID-19 vaccines, Biomed. Pharmacother. 136 (2021), https://doi.org/10.1016/j.biopha.2021.111272.
[11] F. Tian, B. Tong, L. Sun, S. Shi, B. Zheng, Z. Wang, X. Dong, P. Zheng, Mutation N501Y in RBD of spike protein strengthens the interaction between COVID-19 and its receptor ACE2, bioRxiv 19 (2021), 2021.02.14.431117, https://www.biorxiv.org/content/10.1101/2021.02.14.431117v1.
[12] J. Wise, Covid-19: the E484K mutation and the risks it poses, BMJ (2021) n359, https://doi.org/10.1136/bmj.n359.
[13] J.Y. Chung, M.N. Thone, Y.J. Kwon, COVID-19 vaccines: the status and perspectives in delivery points of view, Adv. Drug Deliv. Rev. 170 (2021) 1–25, https://doi.org/10.1016/j.addr.2020.12.011.
[14] D. Weissman, M. Alameh, T. De Silva, B.F. Haynes, B. Korber, D.C. Montefiori, D. Weissman, M. Alameh, T. De Silva, P. Collini, H. Hornsby, R. Brown, D614G spike mutation increases SARS CoV-2 susceptibility to neutralization ll ll short article D614G spike mutation increases SARS CoV-2 susceptibility to neutralization, Cell Host Microbe 29 (2021) 23–31, https://doi.org/10.1016/j.chom.2020.11.012.
[15] L.C. Karlsson, A. Soveri, S. Lewandowsky, L. Karlsson, H. Karlsson, S. Nolvi, M. Karukivi, M. Lindfelt, J. Antfolk, Fearing the disease or the vaccine: the case of COVID-19, Pers. Indiv. Differ. 172 (2021) 110590, https://doi.org/10.1016/j.paid.2020.110590.
[16] Y. Chen, L. Qiu, X. Lin, X. Ke, G. Chen, Infection prevention and control in flight in the COVID-19 vaccine passport era Yufang, Soc. Sci. Res. Netw. (2021).
[17] J. Sitjar, J. Der Liao, H. Lee, H.P. Tsai, J.R. Wang, P.Y. Liu, Challenges of SERS technology as a non-nucleic acid or -antigen detection method for SARS-CoV-2 virus and its variants, Biosens. Bioelectron. 181 (2021) 113153, https://doi.org/10.1016/j.bios.2021.113153.
[18] S.Y. Ding, E.M. You, Z.Q. Tian, M. Moskovits, Electromagnetic theories of surface-enhanced Raman spectroscopy, Chem. Soc. Rev. 46 (2017) 4042–4076, https://doi.org/10.1039/c7cs00238f.
[19] Y.Y. Lin, J. Der Liao, Y.H. Ju, C.W. Chang, A.L. Shiau, Focused ion beam-fabricated Au micro/nanostructures used as a surface enhanced Raman scattering-active substrate for trace detection of molecules and influenza virus, Nanotechnology 22 (2011), https://doi.org/10.1088/0957-4484/22/18/185308.
[20] K. Kim, L. Kashefi-Kheyrabadi, Y. Joung, K. Kim, H. Dang, S.G. Chavan, M.H. Lee, J. Choo, Recent advances in sensitive surface-enhanced Raman scattering-based lateral flow assay platforms for point-of-care diagnostics of infectious diseases, Sensor. Actuator. B Chem. 329 (2021) 129214, https://doi.org/10.1016/j.snb.2020.129214.
[21] J.E. Sanchez, S.A. Jaramillo, E. Settles, J.J. Velazquez Salazar, A. Lehr, J. Gonzalez, C. Rodríguez Aranda, H.R. Navarro-Contreras, M.O. Raniere, M. Harvey, D.M. Wagner, A. Koppisch, R. Kellar, P. Keim, M. Jose Yacaman, Detection of SARS-CoV-2 and its S and N proteins using surface enhanced Raman spectroscopy, RSC Adv. 11 (2021) 25788–25794, https://doi.org/10.1039/d1ra03481b.
[22] J. Sitjar, J.-D. Liao, H. Lee, B.H. Liu, W. Fu, SERS-active substrate with collective amplification design for trace analysis of pesticides, Nanomaterials 9 (2019) 664, https://doi.org/10.3390/nano9050664.
[23] C.W. Chang, J. Der Liao, H.C. Chang, L.K. Lin, Y.Y. Lin, C.C. Weng, Fabrication of nano-indented cavities on Au for the detection of chemically-adsorbed DTNB molecular probes through SERS effect, J. Colloid Interface Sci. 358 (2011) 384–391, https://doi.org/10.1016/j.jcis.2011.03.032.
[24] X.P. Wang, B. Walkenfort, M. König, L. König, S. Kasimir-Bauer, S. Schlücker, Fast and reproducible iSERS microscopy of single HER2-positive breast cancer cells using gold nanostars as SERS nanotags, Faraday Discuss 205 (2017) 377–386, https://doi.org/10.1039/c7fd00135e.
[25] D.K. Singh, E.O. Ganbold, E.M. Cho, C.M. Lee, S.I. Yang, S.W. Joo, Tautomerism of a thiabendazole fungicide on Ag and Au nanoparticles investigated by Raman spectroscopy and density functional theory calculations, J. Mol. Struct. 1049 (2013) 464–472, https://doi.org/10.1016/j.molstruc.2013.06.060.
[26] C. Carlomagno, D. Bertazioli, A. Gualerzi, S. Picciolini, P.I. Banfi, A. Lax, E. Messina, J. Navarro, L. Bianchi, A. Caronni, F. Marenco, S. Monteleone, C. Arienti, M. Bedoni, COVID-19 salivary Raman fingerprint: innovative approach for the detection of current and past SARS-CoV-2 infections, Sci. Rep. 11 (2021) 1–13, https://doi.org/10.1038/s41598-021-84565-3.
[27] B. Robson, COVID-19 Coronavirus spike protein analysis for synthetic vaccines, a peptidomimetic antagonist, and therapeutic drugs, and analysis of a proposed achilles' heel conserved region to minimize probability of escape mutations and drug resistance, Comput. Biol. Med. 121 (2020).